2014 IEEE International Conference on Robotics & Automation (ICRA)
Hong Kong Convention and Exhibition Center
May 31 - June 7, 2014. Hong Kong, China

Optimizing Curvature Sensor Placement for Fast, Accurate Shape Sensing of Continuum Robots

Beobkyoon Kim, *Member, IEEE*, Junhyoung Ha, *Member, IEEE*, Frank C. Park, *Fellow, IEEE* and Pierre E. Dupont, *Fellow, IEEE*

***Abstract*— Robot control requires the rapid computation of robot shape, which for continuum robots typically involves solving complex mechanics-based models. Furthermore, shape computation based on kinematic input variables can be inaccurate due to parameter errors and model simplification. An alternate approach is to compute the shape in real-time from a set of sensors positioned along the length of the robot that provide measurements of local curvature, e.g., optical fiber Bragg gratings. This paper proposes a general framework for selecting the number and placement of such sensors with respect to arclength so as to compute the forward kinematic solution accurately and quickly. The approach is based on defining numerically-efficient shape reconstruction models parameterized by sensor number and location. Optimization techniques are used to find the sensor locations that minimize shape and tip error between a reconstruction model and a mechanics-based model. As a specific example, several reconstruction models are proposed and compared for concentric tube robots. These results indicate that the choice of reconstruction model as well as sensor placement can have a substantial effect on robot shape estimation.**

I. Introduction

Many approaches to robot control involve solving the forward kinematics problem in real-time as a means to compute the desired twist (velocity) vector for the tip coordinate frame. For robots comprised of rigid links and discrete joints, the kinematic model is composed of algebraic equations and is trivial to compute. Continuum robots, however, that obtain their shape through flexure of their structural components, often require more complex mechanics-based models [1], [2], [3] and [4].

For example, the kinematics of concentric tube robots are modeled by a boundary value problem [1], [4]. These models can be difficult to compute in real-time. Furthermore, continuum robots flex when they apply forces to their environment. Accounting for this flexure adds even more complexity to the model [2], [4], [5] and, in addition, sensing is needed to measure flexion.

Approaches to measuring the shape of a continuum robot include image-based methods [6],[7], electromagnetic tracking [8] and force sensing in control tendons [2]. While each of these approaches can be useful in certain circumstances, they can also pose challenges. For example, image-based methods can be computationally intensive leading to low update rates. Electromagnetic tracking is subject to magnetic field distortions and often only provides robot tip location and not robot shape. Tendon force sensing is corrupted by tendon sliding friction and also does not provide local shape information.

B. Kim, J. Ha and F.C. Park are with the School of Mechanical Engineering, Seoul National University, Seoul, Korea. P. E. Dupont is with the Department of Cardiovascular Engineering, Boston Children's Hospital, Harvard Medical School, Boston, Massachusetts, USA.

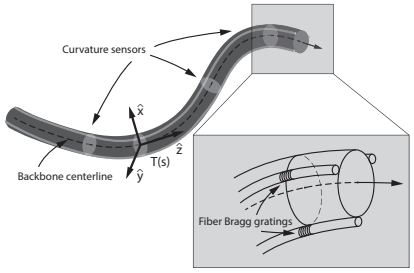

Fig. 1. Fiber Bragg Gratings used as curvature sensors along the length of a continuum robot.

An alternative approach used to measure needle deflection [9], [10] and also recently for continuum robot shape estimation [11] is to use optical fibers with fiber Bragg gratings (FBGs). By arranging multiple fibers (typically three or four) around the circumference of a cylinder at fixed distance from the neutral axis of bending, the strain-induced frequency shift in a set of FBGs can be used to compute the x and y curvature of a cross section. This is shown in Fig. 1. By including multiple FBGs along the length of a fiber, each possessing its own center frequency, the curvature at a discrete set of points along the length of a curved tubular object can be measured. The estimated shape of the object's centerline as well as its tip location can be reconstructed by integrating these curvature measurements using a model describing how curvature varies between sensors.

In prior work, sensors are placed uniformly along the length and use the k-nearest neighbor interpolation model [9] to reconstruct the curvature functions or use a second order polynomial model for curvature functions and solve for the coefficients from the boundary conditions using one-dimensional beam theory [10].

FBG's represent a promising alternative for continuum robot shape sensing and the cost of optical interrogators used to measure frequency shift has decreased considerably in recent years. In order to provide a basis of comparison between this technology and the alternate approaches described earlier, however, several important issues need be addressed. These include characterizing the dependence of centerline and tip frame error on the reconstruction model used as well as on the number of sensors and their location along the

length of the robot.

The contributions of this paper are to provide a framework for addressing this problem, to propose several types of reconstruction models and to illustrate the use of these models in the context of concentric tube robots. The paper is arranged as follows. The next section introduces the general framework for optimizing sensor locations and proposes three reconstruction models parameterized by a set of curvature measurements. Section III applies this framework and the proposed reconstruction models to concentric tube robot kinematics. Numerical examples are presented in Section IV and conclusions appear in final section.

II. Shape Estimation for Continuum Robots

We begin this section with a brief review of the single backbone curve model for describing the kinematics of a general continuum robot. We then discuss shape reconstruction models, and show how optimal sensor locations can be determined via an optimization problem that minimizes the shape and tip errors between the reconstruction model and a mechanics-based model.

A. Kinematics of Continuum Robots

The continuum robots considered in this paper can be modeled by an arclength parametrized curve in three-dimensional space, referred to as the backbone curve. Letting s denote the arclength parameter, a right-handed reference frame $T(s) \in SE(3)$ is then attached to each point of the backbone curve in such a way that (i) the z-axis is always tangent to the backbone curve, and (ii) no rotations about the z-axis (or backbone curve) are permitted. A reference frame defined in this way is referred to as a Bishop frame [12]. Taking the left-invariant derivative of $T(s)$ with respect to s, we obtain

$$[V(s)] = T^{-1}\frac{dT}{ds} = \begin{pmatrix} [u(s)] & \nu \\ 0 & 0 \end{pmatrix} \in se(3), \qquad (1)$$

where $u(s)$ is given by $u(s) = \begin{pmatrix} u_x(s) & u_y(s) & 0 \end{pmatrix}^T \in \mathbb{R}^3$. The curve $u(s) \in \mathbb{R}^3$ denotes the angular velocity of the frame $T(s)$ per unit arclength, while $\nu \in \mathbb{R}^3$ denotes the linear velocity of the origin of $T(s)$ per unit arclength; for the Bishop frame as defined, the z-component of $u(s)$ is zero, and $\nu = \begin{pmatrix} 0 & 0 & 1 \end{pmatrix}^T \in \mathbb{R}^3$.

B. Shape Reconstruction Models

The estimation of shape begins with the reconstruction of the curvature function $\tilde{u}(s)$ defined along the backbone curve (the tilde is used to denote functions defined in terms of the reconstruction model). The coordinate frames $\tilde{T}(s)$ are obtained by integrating Eq. (1). The shape of the robot $\tilde{p}(s)$ can then be obtained by taking the position vector of $\tilde{T}(s)$.

1) Piecewise Constant Curvature Model: Given p sensors with respective locations $s_k \in \mathbb{R}, i = 1, \ldots, p$, the simplest reconstruction method assumes that the curvature between sensors is constant; this implies that the function $\tilde{u}(s)$ is of the form

$$\tilde{u}(s) = u^k = \begin{pmatrix} u_x^k & u_y^k & 0 \end{pmatrix}^T \qquad (2)$$

for $\beta s_{k-1} + (1-\beta)s_k \leq s < \beta s_k + (1-\beta)s_{k+1}$, where u_x^k and $u_y^k \in \mathbb{R}$ respectively denote the bending curvature sensor values at sensor location s_k in the x and y directions. The constant scalar $\beta \in [0, 1]$ controls how the intervals are spaced around the sensor locations: if $\beta = 0$, the sensor covers the interval from its current location to the next sensor, whereas if $\beta = 1$, the sensor covers the interval from the previous sensor location to its current location. The backbone coordinate frame $\tilde{T}(s)$ is computed as follows when β is set to 0:

$$\tilde{T}(s) = T_0 e^{[V_{s_0}](s_1 - s_0)} e^{[V_{s_1}](s_2 - s_1)} \cdots e^{[V_{s_k}](s - s_k)} \qquad (3)$$

The term $[V_{s_k}] \in se(3)$ is given by $[V_{s_k}] = \begin{pmatrix} [u^k] & \nu \\ 000 & 0 \end{pmatrix}$.

2) Basis Function Model: The shape reconstruction models introduced in this paper are based on the assumption that the curvature functions $u(s)$ can be reconstructed as a linear combination of a certain set of basis functions. Consider that the x and y components of $\tilde{u}(s)$ are given in the form

$$\tilde{u}_x(s) = \sum_{j=1}^{q} c_x^j B_x^j(s),\ \tilde{u}_y(s) = \sum_{j=1}^{q} c_y^j B_y^j(s) \qquad (4)$$

where $B_x^j(s)$ and $B_y^j(s) \in \mathbb{R}$ respectively denote basis functions in the x and y directions, c_x^j and $c_y^j \in \mathbb{R}$ are the corresponding coefficients for the x and y components, and q denotes the total number of basis functions. Assume that the basis functions $B_x^j(s)$, $j = 1, \ldots, q$ in Eq. (4) are given. To determine the coefficients c_x^j, $j = 1, \ldots, q$, we can use the sensor measurements at the arclength location s_k, $k = 1, \ldots, p$. Let $f_k \in \mathbb{R}$ be a scalar-valued function associated with the k-th sensor location, defined as the difference between the curvature value $\tilde{u}_x(s_k)$ computed from a reconstruction model and the sensor measurement u_x^k:

$$f_x^k = \tilde{u}_x(s_k) - u_x^k = \sum_{j=1}^{q} c_x^j B_x^j(s_k) - u_x^k \qquad (5)$$

The c_x^j can be expressed as minimizers to the least-squares criterion involving f_k:

$$\bar{c}_x = \arg\min_{\bar{c}_x} \sum_{k=1}^{p} {f_x^k}^2 = \arg\min_{\bar{c}_x} \|B_x \bar{c}_x - \bar{u}_x\|^2, \qquad (6)$$

where $B_x \in \mathbb{R}^{p \times q}$, $\bar{c}_x \in \mathbb{R}^q$ and $\bar{u}_x \in \mathbb{R}^p$ are given by

$$B_x = \begin{pmatrix} B_x^1(s_1) & B_x^2(s_1) & \cdots & B_x^q(s_1) \\ B_x^1(s_2) & B_x^2(s_2) & & B_x^q(s_2) \\ \vdots & & \ddots & \vdots \\ B_x^1(s_p) & B_x^2(s_p) & & B_x^q(s_p) \end{pmatrix} \qquad (7)$$

$$\bar{c}_x = \begin{pmatrix} c_x^1 & c_x^2 & \cdots & c_x^q \end{pmatrix}^T \qquad (8)$$

$$\bar{u}_x = \begin{pmatrix} u_x^1 & u_x^2 & \cdots & u_x^p \end{pmatrix}^T \qquad (9)$$

The generalized inverse ${B_x}^\dagger$ of B_x can be used to compute the augmented coefficient vector $\bar{c}_x$ as follows:

$$\bar{c}_x = {B_x}^\dagger \bar{u}_x \qquad (10)$$

In general, if $p = q$, a unique solution $\bar{c}_x$ can be obtained as

$$\bar{c}_x = {B_x}^{-1}\bar{u}_x. \tag{11}$$

This results in $f_x^k = 0$ for all $k = 1, \ldots, p$, in which case the reconstruction model reduces to an **interpolation** model. If on the other hand $p > q$, then Eq. (10) leads to the least squares sum of f_k, in which case the reconstruction model reduces to a **regression** model. Having the number of sensors p be smaller than the number of bases q is clearly undesirable. If $p < q$, the solution to Eq. (6) is not uniquely determined, and the reconstructed shape tends to deviate in undesirable ways. The same procedure (5)$\sim$(11) can be applied to the y-component of $\tilde{u}(s)$.

Without any knowledge of the mechanics for the target continuum robot, choosing a suitable basis function to efficiently approximate the shape becomes difficult. Popular choices for the basis function include the polynomial basis

$$B_x^j(s) = s^{j-1},\ j = 1, \ldots, q, \tag{12}$$

as well as the Fourier series basis

$$B_x^j(s) = e^{i\frac{2\pi js}{L}},\ j = -q, \ldots, q. \tag{13}$$

C. Optimal Sensor Location

Given p sensors and a reconstruction model $\tilde{u}(\cdot)$, the sensor locations can be determined as the solution to the following optimization problem:

$$\min_{s_k} w_1 J_1 + w_2 J_2,\ k = 1, \ldots, p, \tag{14}$$

where J_1 and J_2 denote the errors of the shape and tip configurations, respectively, and w_1 and w_2 denote the corresponding weight coefficients. Assume that we have M workspace samples, and denote the kinematic input variables corresponding to the l-th workspace sample by ξ_l. Let $u(s, \xi_l)$ and $p(s, \xi_l)$ denote the corresponding kinematic curvature and backbone centerline solutions for ξ_l as determined from a mechanics-based model. The shape error function J_1 can then be defined with respect to either the curvature or the backbone centerline as follows:

$$J_1 = \sum_{l=1}^{M} \frac{1}{L} \int_0^L \|p(s, \xi_l) - \tilde{p}(s, \xi_l)\|\, ds. \tag{15}$$

Note that $u(s, \xi_l)$ and $p(s, \xi_l)$ can be computed from the appropriate mechanics-based kinematic model for all the workspace samples, while $\tilde{u}(s, \xi_l)$ and $\tilde{p}(s, \xi_l)$ are obtained from the chosen reconstruction model. The tip configuration error J_2 over the M workspace samples can then be defined as

$$J_2 = \sum_{l=1}^{M} d_t(T(L, \xi_l), \tilde{T}(L, \xi_l)), \tag{16}$$

where $d_t : SE(3) \times SE(3) \to \mathbb{R}$ denotes a suitable distance metric between a mechanics-based solution of the tip configuration $T(L)$ and one obtained from the reconstruction model $\tilde{T}(L)$.

The objective function defined in (14) represent the averaged error over the workspace samples. The minimizer to (14) can provide the minimum averaged error, however, it does not guarantee to minimize the maximum error over the workspace samples. If one wants the maximum tip position error over the workspace to be minimized, one can consider an alternative optimization formula given by

$$\min_{s_k} \left(\max_l d_t(T(L, \xi_l), \tilde{T}(L, \xi_l)) \right). \tag{17}$$

Similar formula can be applied to the maximum curvature or position shape error.

III. Case Study: Concentric Tube Robots

Concentric tube robots have recently received considerable attention as a new medical instrument for minimally invasive medical procedures. They are composed of pre-curved elastic tubes that are concentrically arranged. In this section, the proposed shape estimation framework is applied to concentric tube robots. It is assumed that the shape sensors are attached to a sensing tube or rod located inside the innermost robot tube that translates with this robot tube. It is also assumed that the sensing tube is very flexible in bending, but is torsionally stiff so that it bends, but does not twist with the innermost robot tube.

Note that concentric tube robots are particularly challenging since the boundaries of their telescoping sections can slide along the robot centerline with respect to the sensors. To take this into account, the basis functions developed here are parameterized by section extension lengths and sensor locations are optimized over the full range of these extension parameters.

A. Kinematics of Concentric Tube Robots

For the shape computation of a concentric tube robot, the rotated angle $\theta_i(s) \in \mathbb{R}$ and the three-component curvature vector $u_i(s) = \begin{pmatrix} u_{ix}(s) & u_{iy}(s) & u_{iz}(s) \end{pmatrix}^T \in \mathbb{R}^3$ for every i-th tube need to be computed along the arclength parameter s. The mechanics-based kinematic equations for a general concentric tube robot with n tubes are derived in [1]; these are of the form

$$\begin{aligned}
\frac{d\alpha_i}{ds} &= u_{iz} - u_{1z},\ i = 2, \ldots, n \\
u_{1z} &= (1/k_{1z})(k_{2z}u_{2z} + \ldots + k_{nz}u_{nz}) \\
\frac{du_{iz}}{ds} &= (k_{ixy}/k_{iz})\,(u_{ix}\hat{u}_{iy} - u_{iy}\hat{u}_{ix}) \\
u_i|_{x,y} &= \left(\left(\sum_{j=1}^{n} K_j \right)^{-1} R_z^T(\alpha_i) \left(\sum_{j=1}^{n} R_z(\alpha_j) K_j \hat{u}_j \right) \right) \Bigg|_{x,y}
\end{aligned} \tag{18}$$

where the relative twist angle $\alpha_i \in \mathbb{R}$ is defined by $\alpha_i = \theta_i - \theta_1$ and $R(\alpha_k)_z \in SO(3)$ denotes the rotation matrix about the z-axis by α_j. $\hat{u}_i = \begin{pmatrix} \hat{u}_{ix} & \hat{u}_{iy} & \hat{u}_{iz} \end{pmatrix}^T \in \mathbb{R}^3$ and $K_i \in \mathbb{R}^{3\times3}$ denote the pre-curvature vector and the frame-invariant stiffness tensor of i-th tube, respectively, while $k_{ixy} \in \mathbb{R}$ and $k_{iz} \in \mathbb{R}$ are the diagonal components of K_i. The kinematic inputs are the insertion distances L_i and the initial relative twist angles $\theta_i(0)$ for every i-th tube. The shape of the concentric tube robot can be computed by

solving the above boundary value problem for the following given boundary conditions:

$$\alpha_i(0) = \theta_i(0) - \theta_1(0),\ i = 2, \ldots, n \quad (19)$$

$$u_{iz}(L_i) = 0,\ i = 2, \ldots, n, \quad (20)$$

which are obtained from the kinematic input variables L_i and $\theta_i(0)$.

Assume that the curvature functions $u_i(s), i = 1, \ldots, n$ are given from the above split boundary value problem. Since we define the shape of a continuum robot in terms of the Bishop frame attached at each point along the backbone curve, the untwisted curvature function $u(s)$ needs to be computed. Consider the curvature function $u_n(s)$ described with respect to the material coordinate frame attached to the n-th tube; by rotating $u_n(s)$ along the z-axis by the amount of its twisted angle $\theta_n(s)$, the x and y components of $u(s)$ can be obtained as follows:

$$\theta_n(s) = \int_0^s u_{nz}(\sigma)d\sigma \quad (21)$$

$$u(s)|_{x,y} = R_z\left(\theta_n(s)\right) u_n(s)|_{x,y} \quad (22)$$

$$u(s)|_z = 0. \quad (23)$$

The kinematic solution for the bending curvatures $u_{ix}(s)$, $u_{iy}(s)$ in the final equation of (18) can be discontinuous along the arclength, at locations where each tube ends or the pre-curvature of each tube changes discontinuously. The pre-curved shape and insertion length of the tubes determine where these discontinuous points are located. Using these points of discontinuity, the total arclength can be divided into several curvature sections. This discontinuity in the curvature functions should be taken into account during shape estimation of the concentric tube robot. We next address section-based reconstruction models that allow for discontinuous bending curvatures at the boundary of each curvature section, i.e., basis functions are parameterized by section extension length.

B. Section-Based Principal Component Analysis Model

In the previous section we have introduced various choices of bases for the curvature function. Assume that mechanics-based kinematic solutions are available at a large number, M, of workspace samples. Denote the kinematic input variables by $\xi = \{\theta_i(0), L_i\}_{i=1,\ldots,n}$ and the corresponding solutions over the M workspace samples by $\{u_x(s, \xi_l), u_y(s, \xi_l)\}_{l=1,\ldots,M}$ (the subscript l in ξ_l is used to denote the index of the workspace samples).

Since the length of each section as well as the total length varies with the kinematic input variable ξ, we define a new length parameter $\hat{s} \in [0, 1]$ to denote the normalized section length. The normalized locations of the junctions will be fixed with this new length parameter. The reconstructed curvature functions $\tilde{u}_x(\hat{s})$ and $\tilde{u}_y(\hat{s})$ in the x and y directions, along the normalized length parameter $\hat{s}$ with q bases, is given by

$$\tilde{u}_x(\hat{s}) = \sum_{j=1}^{q} c_x^j B_x^j(\hat{s}),\ \tilde{u}_y(\hat{s}) = \sum_{j=1}^{q} c_y^j B_y^j(\hat{s}) \quad (24)$$

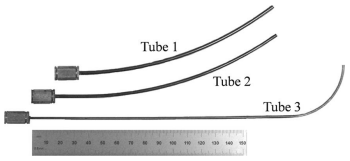

Fig. 2. Three tubes comprising the concentric tube robot design used in the examples. Tubes 1 and 2 form a variable-curvature pair that are rotated with respect to each other to vary their composite curvature. Tube 3 can be arbitrarily rotated and extended and conforms to the curvature of the variable curvature pair when retracted.

where the bases are assumed to be orthogonal:

$$\int_0^1 B^j(\hat{s}) B^{j'}(\hat{s}) d\hat{s} = \begin{cases} 1 & \text{if } j = j' \\ 0 & \text{else} \end{cases} \quad (25)$$

The reconstruction error for the x-curvature function over the normalized length parameter $\hat{s}$ is defined by

$$J_x = \sum_{l=1}^{M} \int_0^1 \|u_x(\hat{s}, \xi_l) - \tilde{u}_x(\hat{s})\|^2 d\hat{s}. \quad (26)$$

Natural bases can be obtained by minimizing J_x with respect to the bases $B_x^l(\hat{s})$:

$$\left\{B_x^1(\hat{s}), \ldots, B_x^q(\hat{s})\right\} = \arg\min_{B_x^l(\hat{s})} J_x. \quad (27)$$

Discretizing every function of $\hat{s}$ in J_x reduces the problem to a vector space minimization corresponding to the well-known principal component analysis.

C. Section-based Polynomial Regression Model

Since the robot has been divided into piecewise continuous curvature sections, the curvature function within each section is guaranteed to be continuous. The simplest bases for continuous functions are polynomials. From observation of the dominant principal components, we can conclude that it is sufficient to use up to quadratic terms as the bases for each section (the number of basis functions q is 3 for the polynomial bases in Eq. (12)):

$$\tilde{u}_x(s) = \begin{cases} c_x^1 & \text{for 1 sensor.} \\ c_x^1 + c_x^2 s & \text{for 2 sensors.} \\ c_x^1 + c_x^2 s + c_x^3 s^2 & \text{for 3 or more sensors.} \end{cases} \quad (28)$$

If a single curvature value is available within the section, the curvature is interpolated by a constant function within the section. If two curvature values are available within the given section, the curvature can be linearly interpolated. If more then two curvature values are available within a given section, the curvature can be interpolated via Eq. (11), or regressed via Eq. (10) to a quadratic function. In the case of no sensor measurements on the given section, the interpolated or regressed function of an adjacent section can be used, although this will likely be inaccurate.

TABLE I

CONCENTRIC TUBE PARAMETERS

	Tube 1	**Tube 2**	**Tube 3**	
	Section 1	Section 1	Section 1	Section 2
Length (mm)	150	150	150	80
Curvature (m^{-1})	4.525	4.525	0.0	16.667
Relative Stiffness	1	1	0.21	0.07

IV. NUMERICAL EXPERIMENTS FOR A CONCENTRIC TUBE ROBOT

In this section we perform numerical experiments to determine how accurately the reconstruction models introduced in Sections II and III can determine the shape of a concentric tube robot. Consider the three-tube design shown in Fig. 2. The model parameters for each tube are given in Table I. This design is described in detail in [1]. Tubes 1 and 2 are a balanced pair of tubes with fixed insertion lengths. The kinematic inputs for this robot are the initial rotated angles $\theta_i(0)_{i=1,2,3}$ of each tube, and the insertion length L_3 of the innermost tube.

For this design, the centerline can be decomposed into three curvature sections by two locations of discontinuous curvature. The first discontinuity occurs at the distal tip of the variable curvature tube pair. The second discontinuity corresponds to the discontinuity in pre-curvature of Tube 3. This location lies in the interior of the variable curvature pair and varies with insertion length, L_3.

We fix the first sensor location at the distal end of the robot ($s = L$). By doing that, we can always measure the curvature of the distal curvature section for the every extension length of Tube 3. For our specific concentric-tube robot, the distal curvature section has always a constant curvature determined by the twisted angle of Tube 3 at the distal.

The three reconstruction models compared here are the piecewise constant curvature model, the section-based PCA model, and the section-based polynomial regression model. For each reconstruction model, results are obtained for two sets of sensor locations: uniformly spaced sensor locations, and the optimized sensor locations obtained as a solution to the optimization problem (14).

To solve for the optimal sensor locations, we use the global optimization toolbox in MATLAB with the interior point algorithm for local search [13] and the scatter-search method for generating trial points [14].

A. Selection of Basis Functions

Basis functions are needed for both the PCA-based model and the polynomial regression model. The PCA basis set can be selected using an eigenvalue analysis of the curvature functions over the workspace to obtain the principal component bases and their corresponding weights. In descending order of the weight values, the first five PC bases are chosen as the basis functions for the section-based PCA model.

As depicted in Fig. 3, the curvature basis functions for $u_x(\hat{s})$ and $u_y(\hat{s})$ can be interpreted geometrically. In particular, the most dominant principal component reproduces the constant pre-curvature of the distal portion of Tube 3. The second most dominant component represents Tubes 1 and 2 as constant in curvature over their length. The third basis elements predominantly model the approximately constant curvature corresponding to the portion of Tube 3 that is retracted into Tubes 1 and 2. The fourth basis elements model the variation from constant curvature of Tubes 1 and 2 as predicted by the mechanics model. The fifth basis elements predominantly model variation in curvature of the portion of Tube 3 that is retracted into Tubes 1 and 2.

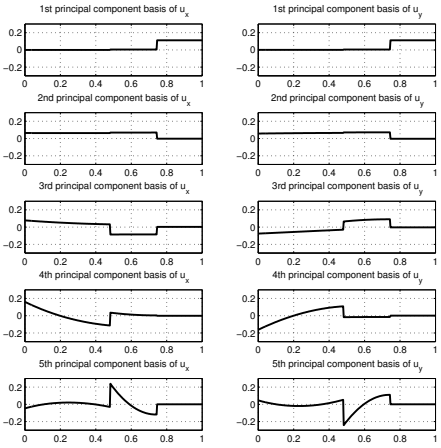

Fig. 3. PCA bases versus normalized section parameters

Selection of basis functions for the section-based polynomial regression model involves choosing the appropriate order of the polynomial. Using the PCA bases as a guide, second order polynomial functions should be sufficient. Thus, the bases described in Section III-C are appropriate for each curvature section.

B. Number and Location of Sensors

Fig. 4 compares the average tip position error over the workspace with respect to the number of sensors 2 to 5. Data for the piecewise constant curvature model is not shown since it is comparatively very large. The solid curves represent the tip position error for the uniformly spaced sensor locations, while the dashed curves are for the optimized sensor locations. When only two sensors are used, the PCA model exhibits the smallest error. As the number of sensors increases, the error of the polynomial model becomes smaller and, while not shown, the errors of both models converge to nonzero lower bounds.

An example of optimized sensor locations is depicted in Fig. 5. In this example, the section-based PCA reconstruction model is used with four sensors. The depicted configuration is when Tube 3 is fully extended such that the middle curvature section has zero arclength. As Tube 3 is retracted, this arclength increases from zero and the optimized location of sensor 2 enables measurement of this middle section's curvature for all possible retraction lengths.

TABLE II

AVERAGE AND MAXIMUM ERROR FOR FIVE SENSORS

	Piecewise Constant Curvature		Section-based PCA		Section-based Polynomial Regression	
	Uniformly Spaced	After Optimization	Uniformly Spaced	After Optimization	Uniformly Spaced	After Optimization
Avg. Tip Position Error (mm)	6.187	3.155	0.343	0.279	0.233	0.044
Max. Tip Position Error (mm)	18.820	14.163	1.838	1.872	1.441	0.527
Avg. Curvature Error (m^{-1})	0.832	0.432	0.044	0.040	0.021	0.004
Max. Curvature Error (m^{-1})	2.267	1.104	0.197	0.210	0.110	0.034
Avg. Backbone Centerline Error (mm)	0.844	0.518	0.062	0.049	0.045	0.009
Max. Backbone Centerline Error (mm)	2.924	2.177	0.327	0.331	0.247	0.098

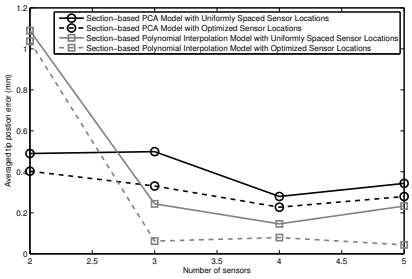

Fig. 4. Average tip position error over the workspace versus the number of sensors.

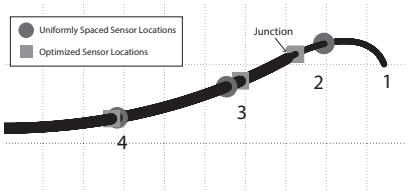

Fig. 5. Optimized and uniformly spaced locations for four sensors using PCA model. Sensor at robot tip is not shown.

C. Comparison between Reconstruction Models

The accuracy of the reconstruction models can be evaluated using the error functions defined in Eqs. (15) and (16): the curvature shape error, the backbone centerline error and the tip position error. Table II lists the average and maximum value of these error functions for the specific case of 5 sensors. The section-based polynomial regression model shows the smallest errors for both uniformly spaced and optimized sensor locations, followed by the section-based PCA model. The piecewise constant curvature model is substantially worse than the other models.

V. CONCLUSION

FBG-based curvature sensing represents a promising approach to real-time shape sensing for continuum robots. The shape reconstruction framework proposed in this paper provides a standardized approach to predicting the accuracy of such a sensing system for any continuum robot whose curvatures are piecewise continuous over sections of varying arclength. Using this framework, reconstruction models can be compared and the number of sensors can be selected to meet specific accuracy requirements. In particular, the numerical experiments presented suggest that, in the case of concentric tube robots, high accuracy can be achieved with a small number of sensors. Current research is extending these results to consider the effects of error inherent in the nominal mechanics-based model as well as error in the curvature sensors.

REFERENCES

[1] P. E. Dupont, J. Lock, B. Itkowitz, and E. Butler, "Design and control of concentric-tube robots," *IEEE Trans. Robotics*, vol. 26, no. 2, pp. 209–225, 2010.

[2] A. Bajo and N. Simaan, "Kinematics-Based Detection and Localization of Contacts Along Multisegment Continuum Robots," *Robotics, IEEE Transactions on*, vol. 28, no. 2, pp. 291–302, 2012.

[3] B. A. Jones and I. D. Walker, "Kinematics for multisection continuum robots," *IEEE Trans. Robotics*, vol. 22, no. 1, pp. 43–55, 2006.

[4] D. C. Rucker, B. A. Jones, and R. J. Webster III, "A geometrically exact model for externally-loaded concentric-tube continuum robots," *IEEE Trans. Robotics*, vol. 26, no. 5, pp. 769–780, 2010.

[5] J. Lock, G. Laing, M. Mahvash, and P. E. Dupont, "Quasistatic modeling of concentric tube robots with external loads," *IEEE/RSJ Int. Conf. Intelligent Robots and Systems*, pp. 2325–2332, 2010.

[6] H. Ren and P. E. Dupont, "Tubular enhanced geodesic active contours for continuum robot detection using 3d ultrasound," pp. 2907–2912, 2012.

[7] E. J. Lobaton, J. Fu, L. G. Torres, and R. Alterovitz, "Continuous shape estimation of continuum robots using x-ray images," *IEEE Int. Conf. Robotics and Automation*, pp. 725–732, 2013.

[8] M. Mahvash and P. E. Dupont, "Stiffness control of continuum surgical manipulators," *IEEE Trans. Robotics*, vol. 27, no. 2, pp. 334–345, 2011.

[9] M. Abayazid, M. Kemp, and S. Misra, "3D Flexible Needle Steering in Soft-Tissue Phantoms using Fiber Bragg Grating Sensors," *IEEE Int. Conf. Robotics and Automation*, pp. 5843–5849, May 2013.

[10] Y.-L. Park, S. Elayaperumal, B. Daniel, S. C. Ryu, M. Shin, J. Savall, R. J. Black, B. Moslehi, and M. R. Cutkosky, "Real-time estimation of 3-d needle shape and deflection for mri-guided interventions," *IEEE/ASME Trans. Mechatronics*, vol. 15, no. 6, pp. 906–915, 2010.

[11] R. Roesthuis, S. Janssen, and S. Misra, "On Using an Array of Fiber Bragg Grating Sensors for Closed-Loop Control of Flexible Minimally Invasive Surgical Instruments," *IEEE/RSJ Int. Conf. Intelligent Robots and Systems*, pp. 2545–2551, November 2013.

[12] R. L. Bishop, "There is more than one way to frame a curve," *Amer. Math. Monthly*, vol. 82, pp. 246–251, March 1975.

[13] R. H. Byrd, M. E. Hribar, and J. Nocedal, "An interior point algorithm for large-scale nonlinear programming," *SIAM Journal on Optimization*, vol. 9, no. 4, pp. 877–900, 1999.

[14] Z. Ugray, L. Lasdon, J. Plummer, F. Glover, J. Kelly, and R. Martí, "Scatter search and local nlp solvers: A multistart framework for global optimization," *INFORMS Journal on Computing*, vol. 19, no. 3, pp. 328–340, 2007.